Received: 26 October 2018 | Revised: 26 January 2019 | Accepted: 28 January 2019 | Published on: 14 May 2019

DOI: 10.1002/gamm.201900012

ORIGINAL PAPER

Biomechanics of the tricuspid annulus: A review of the annulus' in vivo dynamics with emphasis on ovine data

Manuel K. Rausch | **Mrudang Mathur** | **William D. Meador**

Aerospace Engineering and Engineering Mechanics, Biomedical Engineering Institute for Computational Engineering and Sciences, University of Texas at Austin Austin Texas

Correspondence
Manuel K. Rausch, Aerospace Engineering and Engineering Mechanics, Biomedical Engineering, Institute for Computational Engineering and Sciences, University of Texas at Austin, 2501 Speedway, Austin, TX 78712.
Email: manuel.rausch@utexas.edu

Funding information
American Heart Association: 18CDA34120028;

Abstract

The tricuspid annulus forms the boundary between the tricuspid valve leaflets and their surrounding perivalvular tissue of the right atrioventricular junction. Its shape changes throughout the cardiac cycle in response to the forces from the contracting right heart myocardium and the blood-valve interaction. Alterations to annular shape and dynamics in disease lead to valvular dysfunctions such as tricuspid regurgitation from which millions of patients suffer. Successful treatment of such dysfunction requires an in-depth understanding of the normal shape and dynamics of the tricuspid annulus and of the changes following disease and subsequent repair. In this manuscript we review what we know about the shape and dynamics of the normal tricuspid annulus and about the effects of both disease and repair based on noninvasive imaging studies and invasive fiduciary marker-based studies. We further show, by means of ovine data, that detailed engineering analyses of the tricuspid annulus provide regionally resolved insight into the kinematics of the annulus which would remain hidden if limiting analyses to simple geometric metrics.

KEYWORDS

biplane videofluoroscopy, echocardiography, heart valve, magnetic resonance imaging, right ventricle, sonomicrometry, ultrasound

1 | INTRODUCTION

Heart valves ensure unidirectional blood flow through our circulation and, thus, play an undeniably vital role in our cardiovascular system. Depending on their anatomy and location, heart valves are classified as either semi-lunar or atrioventricular. The former are located between the left ventricle and aorta (aortic valve), or the right ventricle and the pulmonary artery (pulmonary valve), while the latter are located between the left atrium and left ventricle (mitral valve), or the right atrium and the right ventricle (tricuspid valve). Their function critically depends on a well-orchestrated interplay between their leaflets and the perivalvular tissue. The boundary of the leaflets, at which they interface with the surrounding tissue, is called the annulus. The annulus is not a clearly distinguishable anatomic structure, but is rather elusively defined as the "hinge region" of the leaflets. Case in point, under echocardiographic imaging, the annulus is most easily identifiable by the relative motion of the leaflets and the tissue of the atrioventricular junction.[1]

During the cardiac cycle, the annuli of each heart valve do not remain static but undergo configurational changes that are driven by the contracting myocardium, the coapting leaflets, and the blood-valve interaction. Much of the interest in the annuli is derived from their shape and dynamics being reflective of the health of their respective heart valve. In fact, changes to either shape or dynamics is strongly correlated with heart valve disease. Consequently, characterization of annular shape and motion

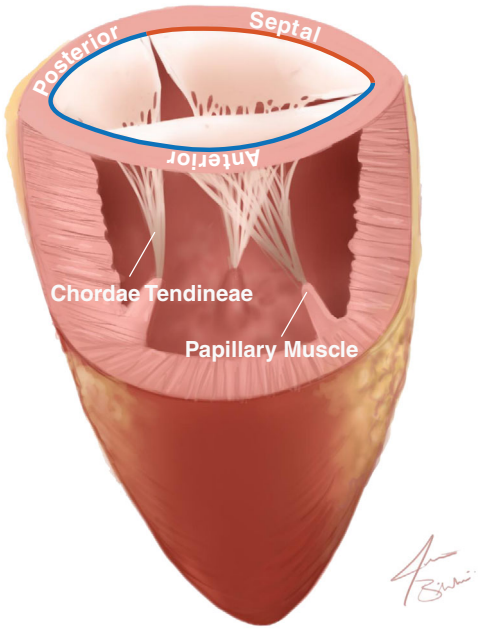

FIGURE 1 Schematic of the right ventricular complex with tricuspid valve leaflets, chordae tendineae, and papillary muscles. The C-shaped, lateral portion of the annulus is highlighted in blue, while the flat, septal annulus is highlighted in red, giving the annulus a D-shaped appearance. Note: The annulus is drawn as a flat structure here, when, in fact, it has a distinct saddle-like shape as we will see later

has become a diagnostic and prognostic clinical tool, and therapeutic strategies for heart valve disease aim at reestablishing the annuli's normal state. Hence, in-depth analyses of annular motion in normal heart valves, diseased heart valves, and repaired heart valves are critical to the successful treatment of heart valve disease. The goal of this article is to review what we know about the annular biomechanics of the tricuspid valve, a valve that has been termed "the forgotten valve" and only now is beginning to receive the appropriate degree of attention given the population's high prevalence of tricuspid valve disease.[2,3]

2 | TRICUSPID VALVE ANATOMY, DISEASE, AND REPAIR

The tricuspid valve, like all other heart valves, essentially functions like a check valve. Its role is to prevent leakage or regurgitation from the right ventricle into the right atrium. Fulfilling this function requires a precisely timed interplay between the three valve leaflets, the valve annulus, and the valve chordae tendineae attached to papillary muscles (see Figure 1). During diastole, when the right ventricle is filling, the valve's function is to minimize the transvalvular pressure gradient. In other words, during diastole, the valve leaflets are pushed out of the way to allow for complete ventricular filling. As the right ventricle contracts during systole, the transvalvular pressure gradient reverses its sign and begins driving blood out of the ventricle. With increasing gradient, the valve leaflets are forced into their closing position where they coapt with each other, thus, creating a seal and occluding the tricuspid orifice. Subsequently, the blood is ejected through the pulmonary valve into the pulmonary arteries and to the lungs. The chordae tendineae that connect the leaflets to the right ventricular endocardium via the papillary muscles, prevent leaflet prolapse into the right atrium. Hence, they function similarly to parachute cords.[4,5]

2.1 | Tricuspid regurgitation

The tricuspid valve can fail in two ways. Either it fails to minimize the transvalvular pressure gradient during diastole, that is, it opposes right ventricular filling, or it fails to maximize the transvalvular gradient during systole, that is, it allows backflow from the right ventricle into the right atrium. The former is known as tricuspid valve stenosis, which is not very common clinically. The latter is referred to as tricuspid regurgitation and is extremely common.[6] Thus, most research on tricuspid valve mechanics has focused on tricuspid regurgitation. In fact, a very large percentage of the population has some degree of tricuspid valve leakage. In the United States, for example, an estimated 82%-86% of the population shows some signs of regurgitation.[7] Obviously, such "trace" amounts of regurgitation are clinically insignificant. However, larger degrees of regurgitation, classified as "moderate to severe" and "severe," are associated with significant morbidity and mortality.[8] The most common causes of tricuspid valve regurgitation are "functional" in nature, meaning that the valve components themselves are intact, but valve-external

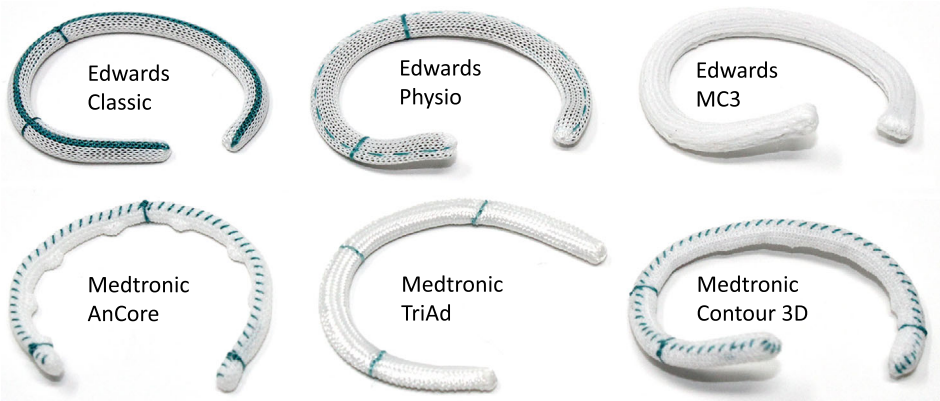

FIGURE 2 Representative tricuspid annuloplasty devices with various degrees of stiffness and three-dimensionality. Note, all devices are shown from a ventricular perspective. Typically these devices exhibit an incomplete ring shape that spares the AV node in the proximity of the septal annulus

factors inhibit proper valve function.[9] For instance, in a large percentage of patients tricuspid valve regurgitation is secondary to mitral valve disease. In those patients, leakage of the mitral valve increases pulmonary pressure, consequently increasing right ventricular pressure. Increased right ventricular pressure ultimately results in ventricular remodeling, papillary muscle displacement, and annular dilation. The displaced papillary muscles, via the chordae tendineae, tether the tricuspid leaflets and hinder their normal motion, while annular dilation increases the transvalvular orifice area and thus competes with the primary valve function. Together, restricted leaflet motion and increased orifice area allow for blood to leak through the valve during right ventricular systole.[10]

2.2 | Tricuspid annuloplasty

Because of this strong correlation between left-sided valve disease and tricuspid valve regurgitation, historically, the tricuspid valve was not repaired.[11] Instead, it was hoped that reverse remodeling following left-sided valve repair would alleviate tricuspid valve disease. To date, surgeons are more aggressive and, when indicated, surgically repair the tricuspid valve during concomitant mitral valve surgery. During tricuspid valve surgery, the valve is generally repaired through either of two techniques: (a) suture-based techniques such as the Kay[12] or DeVega technique,[13] or (b) implantation of tricuspid annuloplasty devices (see Figure 2). The former techniques are simple and inexpensive, but have not withstood the test of time. In fact, recent data very strongly suggest that the latter technique, tricuspid annuloplasty via implantation of annuloplasty devices, is the preferable technique.[14]

Tricuspid annuloplasty devices are incomplete rings that are meant to reinforce and reestablish normal annular size and shape; they vary in three key parameters: size, stiffness, and height. There is relatively little consistency between different devices and the optimal combination of these three design parameters has not yet been determined. As a result, tricuspid valve repair via tricuspid annuloplasty device implantation is far from optimal with failure rates between 10% and 30% on 5-year follow up.[15–17] Optimization of these devices critically requires an in-depth understanding of normal, diseased, and postrepaired annular dynamics.

2.3 | Anatomy of the tricuspid annulus

The gross anatomy of the right atrioventricular junction reveals an asymmetrically shaped geometry of the tricuspid annulus. Its septal portion has little curvature and has been described as "flat" or "straight," while the lateral portion, which is associated with the right ventricular free wall, has a distinct "C-shape." Thus, in its entirety, the gross planar shape of the tricuspid annulus appears to be a "D-shape." As we will see later, the tricuspid annulus is nonplanar in vivo with a distinct three-dimensional (3D) configuration.

Albeit, historically referred to as the "fibrous" annulus, numerous anatomic studies have demonstrated that the tricuspid annulus, in contrast to the mitral annulus, is not fibrous along most of its circumference.[18,19] Instead, only the septal portion demonstrates a distinct fibrosity, while the remainder of the annulus is noncollagenous and primarily composed of coronary vessels and the adipose tissue of the atrioventricular junction that ensures electrophysiological insulation.[20] This heterogeneous composition of the tricuspid annulus may be critical to our understanding of annular dilation in tricuspid valve disease. It has

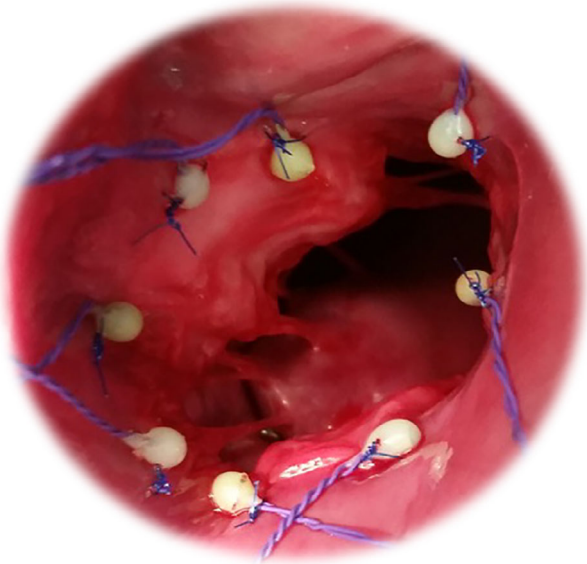

FIGURE 3 Intraoperative image of the ovine tricuspid annulus with eight 2 mm sonomicrometry crystals implanted along its circumference. Each crystal is attached to blue wires and sewn onto the annulus with 4-0 prolene sutures

been suggested that the smaller stiffness of the lateral portion makes it more susceptible to dilation, which consequently increases tricuspid orifice area and reduces coaptation competence (ie, the ability of the leaflets to cover the orifice area to prevent leakage). Thus, the nonfibrous character of the lateral annulus may be a critical driver of valve incompetence and therefore a potential prime target for surgical repair. Additionally, because of its perceived stiffness, the septal annulus has been suggested to provide an appropriate indicator for the normal, nondilated size of the tricuspid valve and thus be used as a device sizing metric during surgical repair.

3 | DYNAMICS OF THE TRICUSPID ANNULUS

Anatomic and histological studies of the tricuspid annulus have been vital for our basic understanding of its composition. However, postmortem studies obviously provide no insight into the dynamic nature of the annulus during the cardiac cycle. Furthermore, in its noncontractile state, the heart changes its gross shape. Thus, ex vivo studies also fail to provide accurate descriptions of the in vivo shape of the annulus. To overcome the shortcomings of ex vivo studies, two lines of research have been pursued that provide insight into the in vivo shape and dynamics of the tricuspid annulus: (a) human studies via noninvasive imaging modalities, that is, ultrasound (US) and magnetic resonance imaging (MRI), (b) large animal studies via fiduciary marker-based techniques. Noninvasive imaging provides the advantage of access to human data, while also being advantageous by requiring no surgery, and thus no disruption of the native state of the tissue. Invasive, fiduciary marker-based techniques are advantageous as they allow for tracking of specific anatomic landmarks, not just throughout a few cardiac cycles, but also between induced disease states and surgical treatments, for example. Thus, they allow calculating accurate mechanical metrics of tissue deformation driven by disease and surgery. In the following section, we describe the primary research methodologies used for in vivo studies of the tricuspid annulus before reviewing the dynamics of the normal, the diseased, and the repaired tricuspid annulus.

3.1 | Research methods

3.1.1 | Annular reconstruction from noninvasive imaging

Before the invention of 3D US, noninvasive studies of the tricuspid annulus relied on manual manipulation of the US probe to allow for sequential 2D imaging at varying orientations. The echocardiographers would then, in each sequential image, identify the position of the tricuspid annulus and note its location. Because of the need for manual manipulation, the angular resolution of this approach was initially limited to four angles, that is, an angular resolution of 45°.[21] Subsequent studies gradually improved the spatial resolution to 30°,[22] 20°, and eventually 3°.[23] With the advent of 3D US, the resolution of echocardiographic analyses improved markedly which allowed for the first high-fidelity calculations of annular area and height throughout the

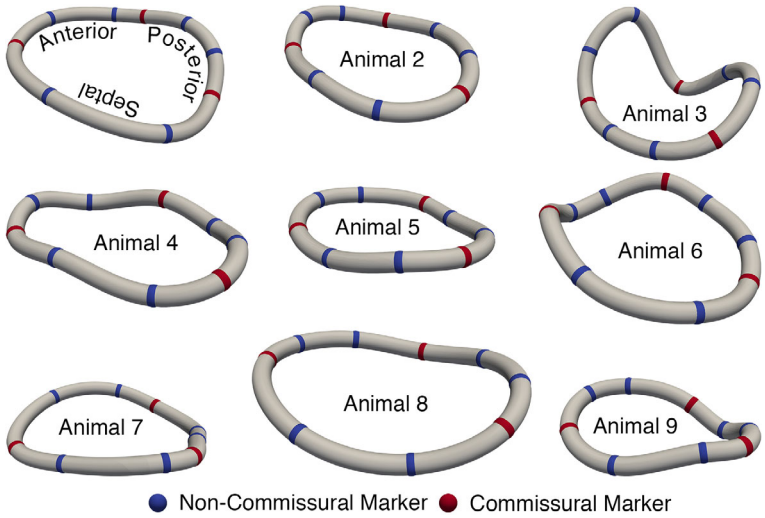

FIGURE 4 Least-squares cubic spline approximations to the tricuspid annuli of nine sheep. The approximations are based on data from nine sonomicrometry crystals at end-diastole. Red markers represent crystals implanted on the commissures, that is, the borders between annular segments, while blue markers are noncommissural. These annuli are all shown to scale and thus illustrate the large variation in size and shape between subjects in vivo. Reproduced with permission from Rausch et al[34]

cardiac cycle.[24–30] Similarly to 3D US, MRI has been used to characterize the 3D configuration of the tricuspid annulus.[31,32] Regardless of imaging technology, the basic approach is identical: points along the annulus are identified in 2D cross-sections and afterwards compiled into 3D point clouds, thus spatially discretizing the annulus. Subsequently, these discrete points are interpolated or approximated using continuous mathematical functions such as piece-wise linear functions, polynomials, splines, and so on. Although, recent technological advancements in both 3D US and MRI now provide sufficiently high spatial and temporal resolution to describe the shape and shape-changes of the annulus accurately, one limitation of these methods is that they cannot track distinct material points. Thus, noninvasive imaging modalities cannot provide kinematic metrics, such as strain along the annulus. In this respect, fiduciary markers provide a significant advantage. Note, that speckle-tracking strain measurements via US have been used to quantify the longitudinal motion of the annulus, or tricuspid annular plane systolic excursion (TAPSE), but not the relative motion along its own length.[33]

3.1.2 | Annular reconstruction from fiduciary markers

In contrast to the above noninvasive approaches, fiduciary marker-based techniques can track discrete points in space and time.[35–39] There are currently two techniques available. The first technique utilizes radiopaque markers that are implanted and subsequently imaged using biplane videofluoroscopy.[40,41] The second technique, which, by now, has essentially replaced the first technique, utilizes so-called sonomicrometry crystals (see Figure 3).[42,43] Each marker houses a piezo crystal that can emit or receive an US signal. Knowing the speed of sound in tissue and by sequentially switching each crystal's function between emitting and receiving, one can determine the distances between all possible marker pair permutations. Once all marker pair distances have been determined, the marker locations can be triangulated using a least-squares approach, for example. This technology is considerably less expensive than a biplane videofluoroscopy setup, is mobile, requires no radiation, and has a higher temporal resolution. However, one limitation of sonomicrometry is that it requires a power source for each crystal, that is, the crystals remain wired even in the beating heart. Additionally, the crystals are relatively large (≥ 0.7 mm). Thus, the inertial impact of wire stiffness and marker weight poses a source of uncertainty in addition to the invasive nature of the procedure. These limitations should be considered when interpreting data discussed in Sections 3.2 to 3.4.

We have previously used both techniques to study the shape and dynamics of the atrioventricular annulus; the former to study the mitral annulus,[37,44–46] and the latter to study the shape and dynamics of the tricuspid annulus.[34,47–49] Regardless of the technique, the end-product is the 3D coordinates of the fiduciary markers.

To transform the fiduciary markers into a continuous mathematical function based on which we are able to calculate kinematic metrics, we have used a least-squares cubic spline-based approach, viz.,

$$\left| \sum_{n=1}^{n_m} \| \chi_n - \boldsymbol{c}_n(s,t) \| + \epsilon \int \left[\partial_s^2 \boldsymbol{c}(s,t) \right]^2 \mathrm{d}s \right| \rightarrow \min, \tag{1}$$

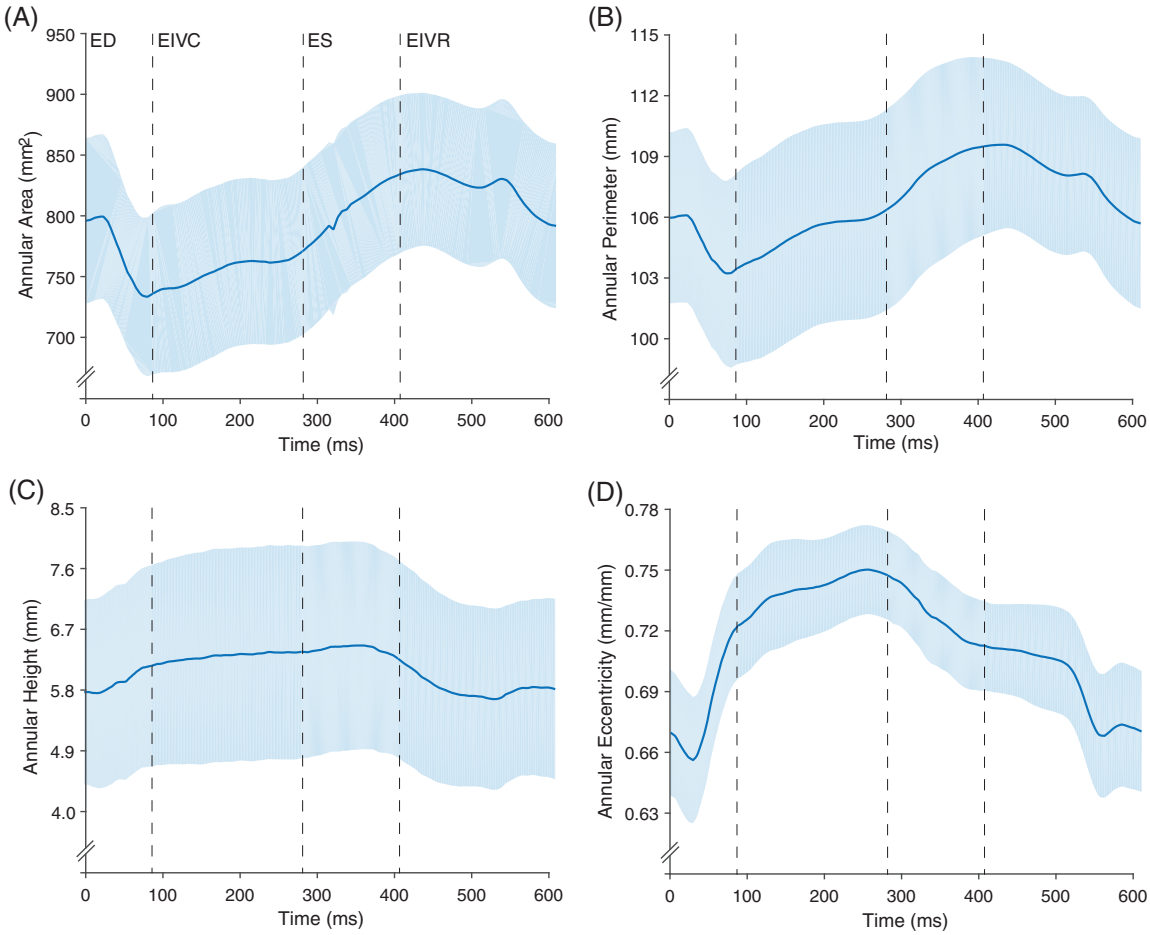

FIGURE 5 Average clinical metrics of annular dynamics among nine sheep reported as mean ± 1 standard error throughout the cardiac cycle, where 0 ms coincides with end-diastole (ED). Other vertical lines indicated end-isovolumetric contraction (EIVC), end-systole (ES), and end-isovolumetric relaxation (EIVR). Reproduced with permission from Rausch et al[34]

where n_m is the total marker number, χ_n are the marker coordinates, $\boldsymbol{c}_n(s,t)$ are the cubic spline segments, and ϵ is a penalty parameter. Thus, the above objective function minimizes the distance between the marker coordinates and the approximating cubic spline function, while penalizing large curvature values. This approach, once calibrated against representative annular data with superimposed synthetic noise, allows for robust approximations of the atrioventricular annulus, while "filtering" out small spatial fluctuations of the markers due to imaging noise (see Figure 4). Upon calculating $\boldsymbol{c}(s,t)$, we may compute displacement fields, strain fields, and curvature fields, for example, as functions of arc-length (s) and time (t). Specifically, we can compute Green-Lagrange strain throughout the cardiac cycle by choosing end-diastole (t_{ED}) as the reference configuration and determining

$$E(s,t) = \left[\lambda(s,t)^2 - 1\right]/2, \tag{2}$$

where $\lambda(s,t)$ is the tangential stretch, that is, $\lambda(s,t) = |\partial_s \boldsymbol{c}(s,t)|/|\partial_s \boldsymbol{c}(s,t_{ED})|$. Similarly, we are able to compute changes in curvature, $\Delta\kappa(s,t)$ between t and t_{ED} as

$$\Delta\kappa(s,t) = \kappa(s,t) - \kappa(s,t_{ED}), \tag{3}$$

where $\kappa(s,\tau)$ is

$$\kappa(s,\tau) = |\partial_s \boldsymbol{c}(s,\tau) \times \partial_s^2 \boldsymbol{c}(s,\tau)|/|\partial_s \boldsymbol{c}(s,\tau)|^3. \tag{4}$$

In the same way that we compute displacements, strains, and changes in curvature throughout the cardiac cycle, we may compute those metrics to characterize the effects of disease and/or repair. To this end, we chose the pre-treatment or control group as the reference configuration and the post-treatment group as the current configuration and compute displacement, strain, and relative curvature between equivalent time points. For example, we compute disease-induced strain by calculating the tangential stretch between t_{ED} after disease and before disease, and repeat this calculation for every time point t of the

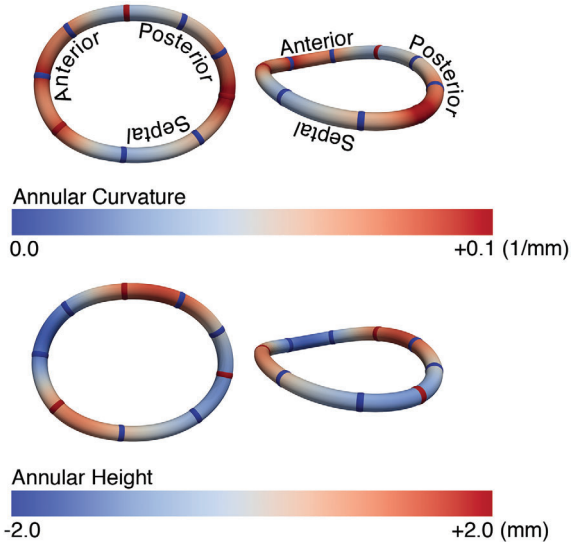

FIGURE 6 Mean values of annular curvature and annular height between nine sheep projected onto a spatially aligned and averaged annulus at end-diastole from an atrial view (left) and an isometric view (right). Annular height was calculated as the normal distance of the annulus from the least-squares plane through the original sonomicrometry crystal locations. Reproduced with permission from Rausch et al[34]

cardiac cycle. To the best of our knowledge, there is only one other group who has chosen a similar, fiduciary marker based approach to compute mechanical metrics of annular dynamics. Eckert et al used higher-order finite elements to interpolate the marker locations along the atrioventricular annulus to compute strain, twist, and bend.[50]

3.2 | The normal annulus

Tsakiris and colleagues[51] were the first to investigate the motion of the tricuspid annulus in vivo. They implanted lead beads around the tricuspid annulus in dogs and tracked their motion throughout the cardiac cycle. Based on biplane videofluoroscopy, as described in Section 3.1.2, they computed the area change of the tricuspid annulus throughout the cardiac cycle. They concluded that the tricuspid annulus is not a static structure, but dynamically deforms by decreasing its area during systole by 29% on average. Thus, the dynamic annular motion aids valve function by decreasing the orifice area during systole and thus supporting the leaflets in valve closure. Additionally, they found that most of the annular area reduction is driven by atrial contraction, not by ventricular contraction. Being an invasive procedure and employing markers of finite weight, this technique is subject to the limitations as discussed in Section 3.1.2. Figure 5 shows the temporal evolution of basic tricuspid annular geometric measurements in detail. Note, this figure is based on sonomicrometry-based measurements in healthy adult sheep.[34]

These findings were corroborated in humans a few years later by Tei et al.[22] Based on multi-angle 2D echocardiography, they found that the tricuspid annulus changes its area dynamically from $11.3 \pm 1.8\,\text{cm}^2$ to $7.6 \pm 1.4\,\text{cm}^2$ during the cardiac cycle, equivalent to an average reduction of 33%. Again, using multi-angle 2D echocardiography, Chandra and colleagues reconstructed the shape of the tricuspid annulus in healthy patients[23] based on a cubic spline reconstruction similar to what we described in Section 3.1.2.[52] Using a higher spatial resolution than Tei et al, they were able to also reconstruct, for the first time, the height profile of the annulus, that is, its out of plane deviation. In addition to the planar dynamic motion described before, they found that the annulus is more "saddle-shaped" during systole than during diastole. Thus, as the annulus contracts during systole, it bends out of plane. However, these data were based on a very small patient population of just two. Thus, no statistically meaningful data was derived from this early study.

The first study to specifically investigate the change in saddle-height throughout the cardiac cycle was due to Hiro et al.[53] Based on fiduciary markers in sheep, they reported on two interesting findings: first, they did not detect a change in saddle-height between systole and diastole, in contrast to Tei et al. Second, they found that the septal aspect of the tricuspid annulus undergoes almost as much change throughout the cardiac cycle as the lateral aspect (anterior + posterior). Specifically, they found the change in the septal annulus to be 10.4% versus 13.0% and 14.0% for the anterior and posterior annulus, respectively. This is interesting as the annulus in the septal region is fibrous while the annulus in the lateral region is nonfibrous. This distinction was assumed to translate to significantly different stiffnesses and thus dynamics throughout the cardiac cycle. Hiro et al's finding may indicate that the higher stiffness of the lateral annulus is overcome by a larger contractile force of the septum, thus, resulting in similar annular shortening despite varying degrees of stiffness.[54]

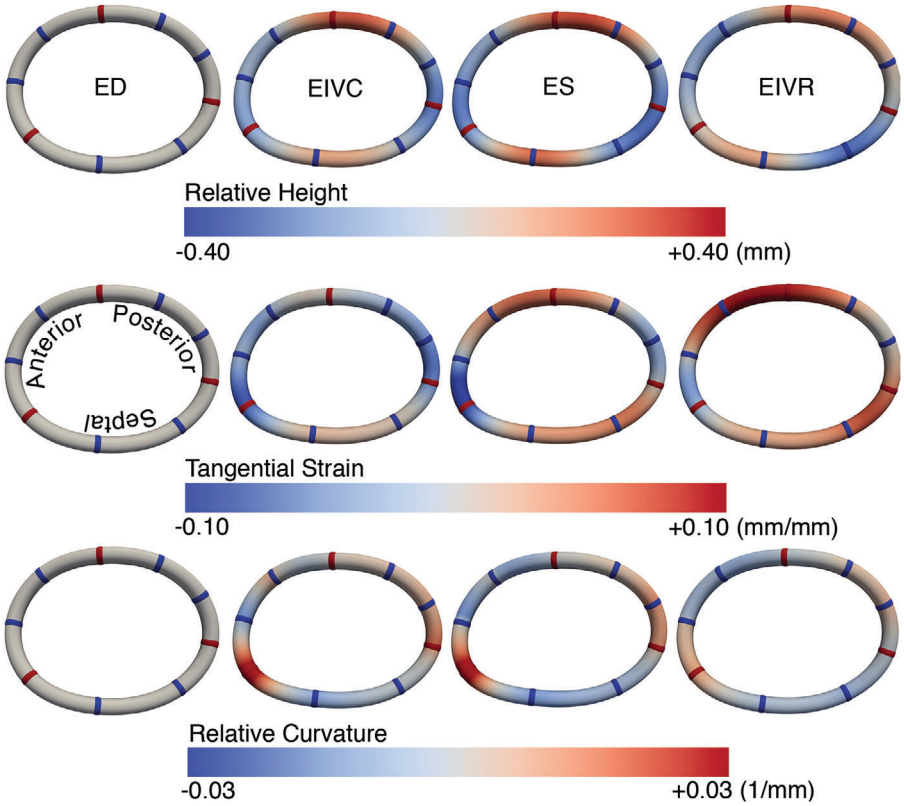

FIGURE 7 Mean values of engineering metrics of annular dynamics between nine sheep projected onto a spatially aligned and averaged annulus at end-diastole (ED), end-isovolumetric contraction (EIVC), end-systole (ES), and end-isovolumetric relaxation (EIVR), relative to ED. Relative height measures the relative change in the normal distance of the annulus to its best-fit plane throughout the cardiac cycle in reference to the height profile at ED. Tangential strain and relative curvature are calculated as per Section 3.1.2. Reproduced with permission from Rausch et al[34]

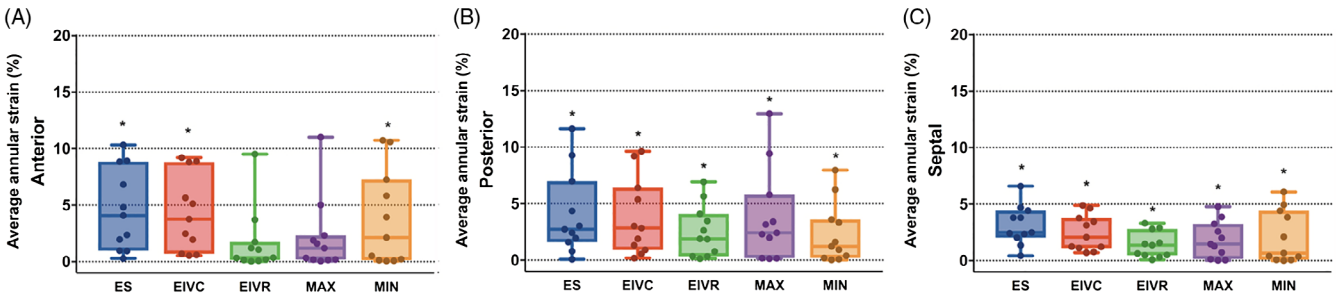

FIGURE 8 Regional annular strains in human beating heart explants based on sonomicrometry and least-squares cubic spline approximations. Strains are shown at end-systole (ES), end-isovolumetric contraction (EIVC), end-isovolumetric relaxation (EIVR), and at the time of maximal (MAX) and minimal (MIN) annular area, all relative to end-diastole. Reproduced with permission from Malinowski et al[49]

The most comprehensive study on human tricuspid annular shape and dynamics was published by Fukuda and colleagues using 3D echocardiography.[24] While essentially reconfirming basic data on annular size and size changes throughout the cardiac cycle, they demonstrate a clear change in annular height between systole and diastole, thus contradicting Hiro et al while corroborating the findings of Chandra et al. Also, using 3D echocardiography, Kwan et al,[27] Ring et al,[26] Owais et al,[55] and Nishi et al[56] and other groups made similar observations.

In contrast to all previous studies, we have recently published two comprehensive studies on normal annular shape and dynamics based on regionally resolved field metrics. Specifically, we based our analyses on nine sonomicrometry crystals implanted around the tricuspid annulus of sheep and ex vivo beating human hearts. As per the least-squares cubic spline-based approach described in Section 3.1.2, in our first study, we characterized the shape of the tricuspid annulus at end-diastole via continuous curvature and height fields (see Figure 6). While re-confirming previous findings on the general shape of the annulus, we were able to spatially resolve the exact origins of the annular shape. For example, we determined that the annular ellipticity is driven by smaller than average curvature along the mid-anterior and posterior-septal regions and larger than average curvature

along the mid-septal and anterior-posterior annulus. Also, the saddle-shape of the tricuspid annulus is due to distinct peaks in height at the anterior-posterior commissure and the anterior-septal commissures.

In Figure 7, we utilized relative height, that is, the height change between all time points of the cardiac cycle relative to end-diastole, tangential strain relative to end-diastole, and relative curvature, that is, the change in curvature between all time points of the cardiac cycle relative to end-diastole to describe normal annular motion. We found that the dynamics of the tricuspid annulus that previously have only been characterized using simple geometric metrics such as area and perimeter, are driven by distinct regional patterns. Specifically, we identified that the dynamic changes in saddle-height described first by Chandra et al,[23] are due to an increase in height at the anterior-posterior annulus and mid-septal annulus. Similarly, we identified the source of area change throughout the cardiac cycle as a heterogeneous shortening of the annulus primarily in the anterior-septal region and the posterior-septal region, and least in the mid-septal region. Finally, the increased ellipticity during systole follows from a highly localized increase in curvature at the anterior-septal annulus and the posterior-septal annulus. Furthermore, we used a commercial organ preservation system to study transplant-rejected, beating human hearts via sonomicrometry. Our findings largely aligned with those in sheep. However, annular dynamics were smaller than reported in sheep and noninvasive imaging studies likely due to the left ventricle not having been loaded and the unnatural boundary conditions on the ventricle, such as the lack of constraint through peri-cardiac tissue.[49] This difference can be observed in Figure 8, where annular strains throughout the cardiac cycle are significantly lower than those reported in Figure 7 based on sheep. Nonetheless, because this is the first framework that was applied to both human and sheep data, this study is an important step toward transferring knowledge from sheep to humans. Similar, future studies that do not suffer from the same limitations will hopefully bridge the gap between animal models and the patient.

3.3 | The diseased annulus

The diseased annulus has been studied using the same techniques as described in Section 3.1. The first study of annular motion in patients with tricuspid valve regurgitation goes back to Tei et al.[22] Using multiangle 2D echocardiography, they found that the tricuspid annulus in patients with tricuspid regurgitation is significantly larger. Specifically, they found that the area increases from $11.3 \pm 1.8\,\text{cm}^2$ to $15.8 \pm 1.8\,\text{cm}^2$. At the same time, they found that the annulus loses its dynamic range, which goes down from 33% in normal patients to 18% in patients with tricuspid regurgitation. Fukuda et al used 3D echocardiography to elaborate on these findings and showed that reduction in annular dynamics correlates with degree of regurgitation. For example, patients with only mild regurgitation presented with an area reduction of 27.1%, moderate regurgitation presented with 25.4% area reduction, and severe regurgitation presented with 14.6% area reduction.[24] Additionally, Fukuda et al reported that patients with tricuspid regurgitation had more planar annuli, that is, annular height was reduced. Furthermore, Ring et al[26] reported on detailed changes in annular dynamics in patients with dilated right hearts. They found that the annulus in dilated hearts becomes more circular but height, in contrast to the findings of Fukuda et al, does not change. It is important to note that they operated with very limited temporal resolution of only three time points during systole which makes it not unlikely that they may have missed peak values. Also, the patient populations between Fukuda et al's study and that of Ring et al were different.

We have recently developed several acute tricuspid regurgitation sheep models to study changes in the dynamics of the diseased annulus.[48,57] In an acute pulmonary hypertension model, for example, we calculated classic clinical metrics of annular dynamics reported in the medical literature, such as annular area, perimeter, height, and eccentricity.[47,58] We compared the temporal evolution of those metrics between the normal annulus and the disease annulus (see Figure 9). These data qualitatively confirm the findings in noninvasive human studies. With pulmonary hypertension, the annulus significantly increases its area and decreases its dynamic change throughout the cardiac cycle. Also, we elucidated that the eccentricity significantly decreases, that is, the annulus becomes more circular. Interestingly, we also did not find any changes in absolute height, or changes in height throughout the cardiac cycle. Differences to Fukuda et al, who did find that the annular height is reduced in diseased hearts, could be explained by our use of an animal model rather than using human data, the use of fiduciary marker-based technique rather than noninvasive imaging, or the fact that we looked at an acute disease model rather than a chronic model.

Beyond these clinical metrics, we also computed tangential strain, relative curvature changes, and relative height changes along the tricuspid annulus at all time points of the cardiac cycle in the same acute pulmonary hypertension disease model, relative to the annulus before disease induction (see Figure 10). We were motivated by explaining the underlying, regionally resolved drivers behind the changes seen in the diseased tricuspid annulus. We illustrated that the dilation of the tricuspid annulus following acute pulmonary hypertension is driven by heterogeneous lengthening of the annulus, primarily in the antero-septal and anterior-posterior regions. Additionally, we found that the circularization of the tricuspid annulus is due to decreasing curvature in the anterior-septal and anterior-posterior regions and an increase in curvature in the remainder of the annulus. Finally, we demonstrated that there were some regional changes in annular height, albeit only marginal ones.

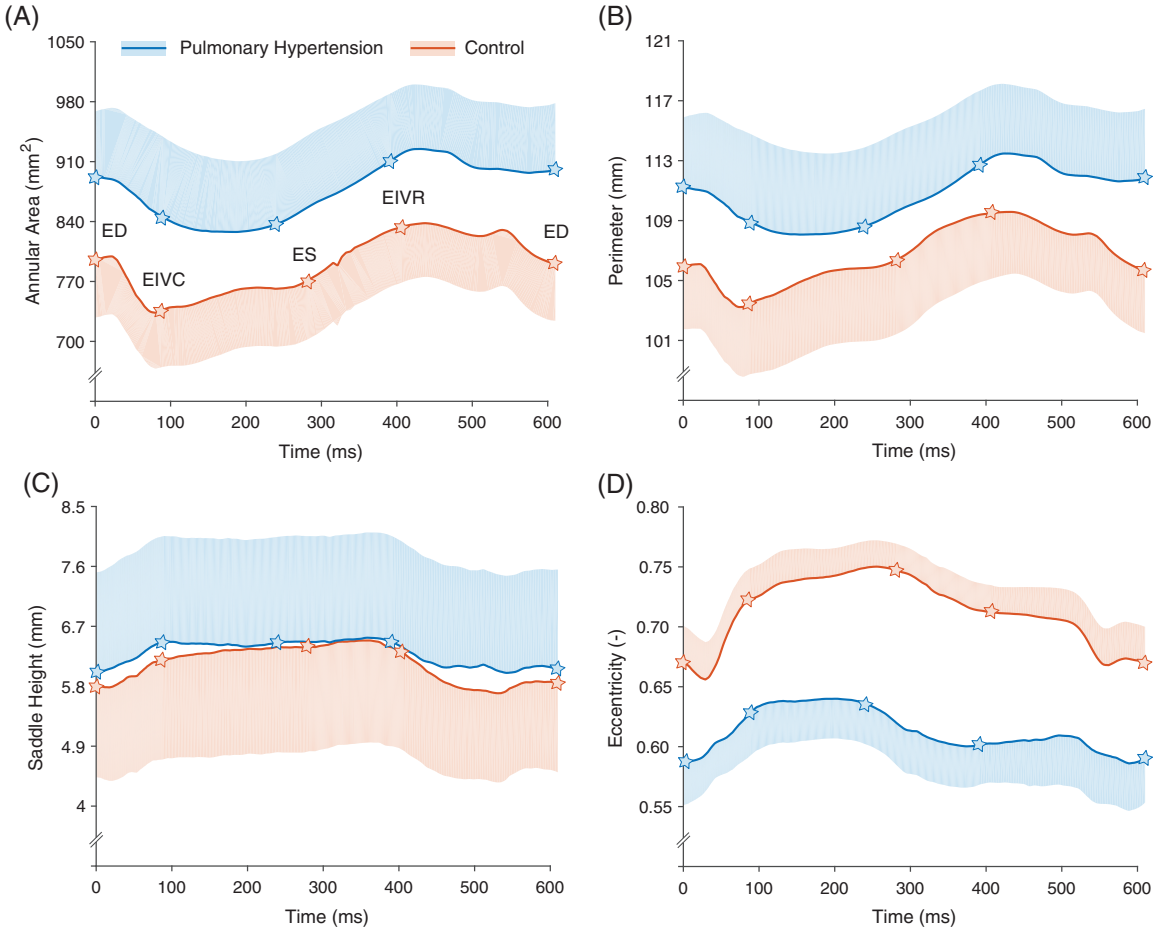

FIGURE 9 Average clinical metrics among nine normal sheep (red) and nine sheep with acute pulmonary hypertension (blue) throughout the cardiac cycle reported as mean ± 1 standard error where 0 ms coincides with end-diastole (ED). Stars indicate end-isovolumetric contraction (EIVC), end-systole (ES), and end-isovolumetric relaxation (EIVR). Reproduced with permission from Rausch et al[47]

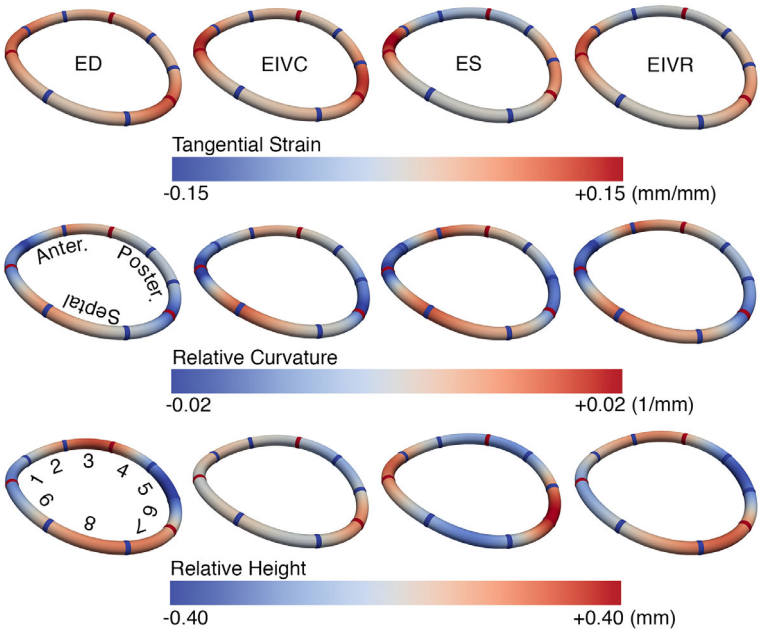

FIGURE 10 Mean values of engineering metrics of annular dynamics projected onto a spatially aligned and averaged annulus at end-diastole (ED), end-isovolumetric contraction (EIVC), end-systole (ES), and end-isovolumetric relaxation (EIVR). Reproduced with permission from Rausch et al[47]

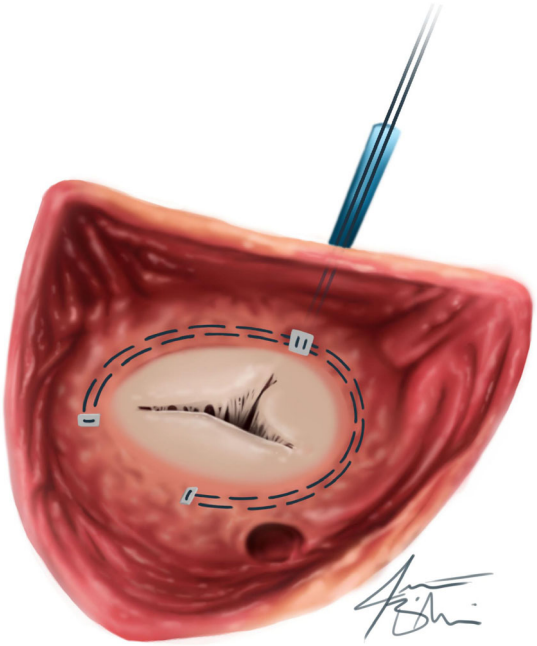

FIGURE 11 Artistic illustration of our suture-based annular cinching technique from an atrial view. Shown are the double row suture (black), pledgets (white), the tricuspid valve leaflets, and the externalized cinch mechanism

3.4 | The repaired annulus

The dynamics of the tricuspid annulus after repair were first investigated by Chandra et al.[23] They used multi-angle 2D echocardiography to quantify annular area in the normal annulus and the annulus of a patient after implantation of a flexible annuloplasty device. They determined that tricuspid annuloplasty via a flexible device preserves some degree of annular dynamics as measured via area change throughout the cardiac cycle. However, their study was only based on one patient and thus carried no statistical relevance. The first analysis of annular dynamics after tricuspid valve repair in a larger patient population goes back to Nishi et al.[56] They compared annular dynamics after implantation of flexible and rigid annuloplasty devices with annular dynamics in healthy control patients. As one would expect, while both devices reduced annular size to normal, dynamics were altered. In agreement with Chandra et al, Nishi et al found that a flexible device largely preserves annular dynamics as measured by area change throughout the cardiac cycle (≈20% in the flexible group versus 30.2% in the control group), while a rigid device diminishes all annular dynamics (≈5% in the rigid group versus 30.2% in the control group).

We recently performed DeVega suture annuloplasty repairs in sheep with acute functional tricuspid regurgitation induced via pulmonary banding, volume overload, and right ventricular ischemia.[48] Figure 11 illustrates our experimental technique in which we placed pledget-supported double row sutures along the lateral annulus and externalized those sutures in anesthetized sheep. By pulling the external sutures, we were able to adjust annular circumference in two consecutive steps of increasing cinching without secondary surgery in a beating ovine heart. As in our previous studies, we used sonomicrometry to calculate classic clinical metrics of annular dynamics, such as annular area and perimeter, throughout the cardiac cycle, before and after annular cinching via suture annuloplasty. We found that suture-annuloplasty, for both degrees of cinching, preserved normal annular dynamics measured as segmental annular length change. Additionally, we computed repair induced changes as tangential strain (see Figure 12). We identified that suture-annuloplasty induces significant compressive strains in the lateral annulus. The magnitude of those strains depended on the degree of cinching. As one would expect, we demonstrated that the septal annulus, which is not covered by the suture annuloplasty, undergoes only marginal compression.[59]

3.5 | The tricuspid annulus in numerical models

With increasing interest in the physiology and pathophysiology of the tricuspid valve there has also been a steadily increasing effort toward numerical models. The very first model of the tricuspid valve was described by Stevanella et al.[60] For the lack of complete, patient-specific data sets, they combined geometric and constitutive information on leaflets and chordae from humans and pigs. The annular geometry of their model was derived from sonomicrometry data, which were collected in sheep by Hiro et al.[53] Moreover, annular dynamics were imposed by means of the same data. Their model was able to produce qualitatively

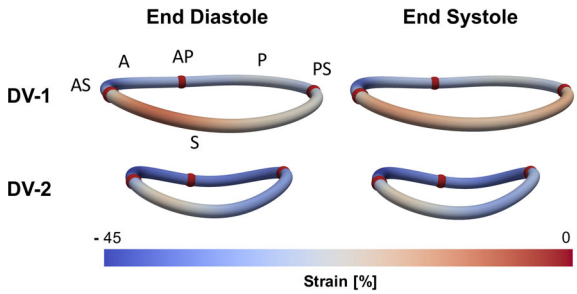

FIGURE 12 Tangential annular strain after suture-based cinching in sheep at end-diastole and end-systole. Strains were calculated relative to the annulus before cinching at the same time points. DV-1 is the first cinching step, while DV-2 is the second cinching step in the same animal. Anatomic landmarks are anterior (A)-septal (S) commissure (AS), anterior-posterior (P) commissure (AP), posterior-septal commissure (PS). These data are based on least-squares cubic spline approximation to sonomicrometry crystal coordinates collected in the beating ovine heart. Reproduced with permission from Malinowski et al[59]

feasible valve geometries under loading. However, given the uncertainty associated with combining data from various sources and species, the quantitative accuracy of their data remains to be confirmed. Kamensky et al, as a numerical example of a novel contact algorithm, performed a similar simulation as Stevanella et al.[61] Here the annular geometry was based on micro CT data on isolated porcine hearts. To the best of our knowledge, the annulus was treated as static in their simulations. Again, as their model was based on a combination of datasets, derived results should be treated with care. Finally, Kong et al, recently introduced the most comprehensive models of human tricuspid valves.[62] Combining in vivo data from human patients with the mechanical properties of unmatched patients, they built three models. In these models the annular geometry and its dynamics were based on CT segmentations. As their models are based on human data only with patient-specific leaflet and annular geometries and realistic annular kinematics, their results are likely the most meaningful to date. These first numerical simulations of tricuspid valve function illustrate the need for detailed information on the shape and dynamics of the tricuspid annulus. More detailed data will, in the future, for example, allow for accurate models of the tricuspid valve toward clinically useful, predictive models of disease progression.

4 | CONCLUSION

The tricuspid annulus is a seemingly simple anatomic structure, yet of complex geometry, and of vital importance. The combination of noninvasive imaging and fiduciary marker-based techniques has provided detailed insight into its shape and dynamics under healthy conditions. Now, we know that the normal annulus is D-shaped with an out-of-plane excursion that gives it the appearance of a saddle. Its physiological in-plane motion may be described as sphincteric, reducing the orifice area from diastole to systole by roughly a third and making it more elliptic. Additionally, it undergoes an out-of-plane configurational change that accentuates its three-dimensionality. These changes are driven by highly localized alterations that can be well-described using displacement, strain, and curvature fields. The most common tricuspid valvular disease is functional tricuspid regurgitation. Under those pathological conditions, the annulus becomes larger, flatter, and more circular. Those changes in shape are accompanied by alterations in its dynamic behavior. Specifically, changes in area throughout the cardiac cycle become less pronounced. However, in contrast to the normal annulus, the diseased annulus has received considerably less attention and there are some conflicting data especially on annular height changes with disease. Even less data is available on the tricuspid annulus and its dynamics after repair. It is understood, however, that annuloplasty via flexible devices and suture-based annuloplasty preserve some degree of annular dynamics, while annuloplasty via rigid devices diminishes all annular dynamics. The consequences of altering annular dynamics are to date unknown. It is important to note that much of the reviewed research was performed in animals. Thus, care must be taken before extrapolating findings to human patients. Future research on annular dynamics should focus on identifying differences between the mechanics of the human annulus and the annulus in animals. Additionally, more effort should be made on characterizing the diseased and repaired tricuspid annulus in the hope of improving currently poor outcomes of tricuspid valve surgery.

ACKNOWLEDGEMENTS

We acknowledge and appreciate the support from the American Heart Association via the Scientist Development Award #18CDA34120028. The authors also acknowledge Jeanette Binkowski for the preparation of Figures 1 and 11.

REFERENCES

[1] M. S. Sacks, A. P. Yoganathan, *Philos. Trans. R. Soc. B: Biol. Sci.* **2007**, *362*, 1369.
[2] J. Mascherbauer, G. Maurer, *Eur. Heart J.* **2010**, *31*, 2841.
[3] C. Bouleti, J. M. Juliard, D. Himbert, B. Iung, E. Brochet, M. Urena, M. P. Dilly, P. Ou, P. Nataf, A. Vahanian, *Arch. Cardiovasc. Dis.* **2016**, *109*, 55.
[4] M. D. Silver, J. H. C. Lam, N. Ranganathan, E. D. Wigle, *Circulation* **1971**, *43*, 333.
[5] J. T. Tretter, A. E. Sarwark, R. H. Anderson, D. E. Spicer, *Clin. Anat.* **2016**, *29*, 399.
[6] P. M. Shah, A. A. Raney, *Curr. Probl. Cardiol.* **2008**, *33*, 47.
[7] J. P. Singh, J. C. Evans, D. Levy, M. G. Larson, L. A. Freed, D. L. Fuller, B. Lehman, E. J. Benjamin, *Am. J. Cardiol.* **1999**, *83*, 897.
[8] A. Mangieri, C. Montalto, M. Pagnesi, R. J. Jabbour, J. Rodés-Cabau, N. Moat, A. Colombo, A. Latib, *Circul. Cardiovasc. Interv.* **2017**, *10*, 1.
[9] G. D. Dreyfus, R. P. Martin, K. M. J. Chan, F. Dulguerov, C. Alexandrescu, *J. Am. Coll. Cardiol.* **2015**, *65*, 2331.
[10] E. M. Spinner, P. Shannon, D. Buice, J. H. Jimenez, E. Veledar, P. J. Del Nido, D. H. Adams, A. P. Yoganathan, *Circulation* **2011**, *124*, 920.
[11] N. S. Braunwald, J. Ross, A. G. Moruow, A. G. Morrow, *Circulation* **1967**, *35*, I63.
[12] J. H. Kay, A. Michael Mendez, P. Zubiate, *Ann. Thorac. Surg.* **1976**, *22*, 498.
[13] P. M. McCarthy, S. K. Bhudia, J. Rajeswaran, K. J. Hoercher, B. W. Lytle, D. M. Cosgrove, E. H. Blackstone, *J. Thorac. Cardiovasc. Surg.* **2004**, *127*, 674.
[14] M. Khorsandia, A. Banerjeeb, H. Singhb, Srivastava, *Interact. Cardiovasc. Thorac. Surg.* **2012**, *15*, 129.
[15] K. Matsuyama, M. Matsumoto, T. Sugita, J. Nishizawa, Y. Tokuda, T. Matsuo, Y. Ueda, *J. Heart Valve Dis.* **2001**, *10*, 520.
[16] K. Onoda, F. Yasuda, M. Takao, T. Shimono, K. Tanaka, H. Shimpo, I. Yada, *Ann. Thorac. Surg.* **2000**, *70*, 796.
[17] S. Fukuda, J. M. Song, A. M. Gillinov, P. M. McCarthy, M. Daimon, V. Kongsaerepong, J. D. Thomas, T. Shiota, *Circulation* **2005**, *111*, 975.
[18] R. H. Anderson, S. Y. Ho, A. E. Becker, *Anat. Rec.* **2000**, *260*, 81.
[19] M. Dudziak, M. Skwarek, J. Hreczecha, J. Jerzemowski, M. Grzybiak, *Folia Morphol* **2009**, *68*, 32.
[20] S. Messer, E. Moseley, M. Marinescu, C. Freeman, M. Goddard, S. Nair, *J. Heart Valve Dis.*, *2012*, 368.
[21] E. Hammarström, B. Wranne, F. J. Pinto, J. Puryear, R. L. Popp, *J. Am. Soc. Echocardiogr.* **1991**, *4*, 131.
[22] C. Tei, J. P. Pilgrim, P. M. Shah, J. A. Ormiston, M. Wong, *Circulation* **1982**, *66*, 665.
[23] S. Chandra, K. Powell, C. S. Breburda, I. Mikic, R. Shekha, A. Morehiead, D. M. Cosgrove, *Comput. Cardiol.* **1996**, 693.
[24] S. Fukuda, G. Saracino, Y. Matsumura, M. Daimon, H. Tran, N. L. Greenberg, T. Hozumi, J. Yoshikawa, J. D. Thomas, T. Shiota, *Circulation* **2006**, *114*, I492.
[25] A. M. Anwar, M. L. Geleijnse, F. J. ten Cate, F. J. Meijboom, *Interact. Cardiovasc. Thorac. Surg.* **2006**, *5*, 683.
[26] L. Ring, B. S. Rana, A. Kydd, J. Boyd, K. Parker, R. A. Rusk, *Eur. Heart J. Cardiovasc. Imag.* **2012**, *13*, 756.
[27] J. Kwan, G. C. Kim, M. J. Jeon, D. H. Kim, T. Shiota, J. D. Thomas, W. H. Lee, *Eur. J. Echocardiogr.* **2007**, *8*, 375.
[28] Z. O. Knio, M. Montealegre-Gallegos, L. Yeh, B. Chaudary, J. Jeganathan, R. Matyal, K. R. Khabbaz, D. C. Liu, V. Senthilnathan, F. Mahmood, *Ann. Cardiac Anaest.* **2016**, *19*, 599.
[29] L. P. Badano, E. Agricola, L. P. de Isla, P. Gianfagna, J. L. Zamorano, *Eur. J. Echocardiogr.* **2009**, *10*, 477.
[30] S.-Y. Min, J.-M. Song, J.-H. Kim, M.-K. Jang, Y.-J. Kim, H. Song, D.-H. Kim, *Eur. Heart J.* **2010**, *31*, 2871.
[31] S. Leng, M. Jiang, X. D. Zhao, J. C. Allen, G. S. Kassab, R. Z. Ouyang, J. Le Tan, B. He, R. S. Tan, L. Zhong, *Ann. Biomed. Eng.* **2016**, *44*, 3522.
[32] F. Maffessanti, P. Gripari, G. Pontone, D. Andreini, E. Bertella, S. Mushtaq, G. Tamborini, L. Fusini, M. Pepi, E. G. Caiani, *Eur. Heart J. Cardiovasc. Imag.* **2013**, *14*, 986.
[33] T. Shen, M. H. Picard, L. Hua, S. M. Burns, M. N. Andrawes, *Anesth. Analg.* **2018**, *126*, 62.
[34] M. K. Rausch, M. Malinowski, P. Wilton, A. Khaghani, T. A. Timek, *Ann. Biomed. Eng.* **2017**, *9*, 365.
[35] J. H. Gorman, R. C. Gorman, B. M. Jackson, Y. Enomoto, M. G. S. John-Sutton, L. Henry Edmunds, *Ann. Thorac. Surg.* **2003**, *76*, 1556.
[36] H. Fawzy, K. Fukamachi, C. D. Mazer, A. Harrington, D. Latter, D. Bonneau, L. Errett, *J. Thorac. Cardiovasc. Surg.* **2011**, *141*, 1037.
[37] M. K. Rausch, W. Bothe, J. P. E. Kvitting, J. C. Swanson, D. C. Miller, E. Kuhl, *Ann. Biomed. Eng.* **2012**, *40*, 750.
[38] M. Malinowski, P. Wilton, A. Khaghani, M. Brown, D. Langholz, V. Hooker, L. Eberhart, R. L. Hooker, T. A. Timek, *Interact. Cardiovasc. Thorac. Surg.* **2016**, *23*, 391.
[39] W. D. Meador, M. Malinowski, T. Jazwiec, M. Goehler, N. Quay, T. A. Timek, M. K. Rausch, *J. Biomech.* **2018**, *80*, 179.
[40] M. K. Rausch, W. Bothe, J. P. E. Kvitting, S. Göktepe, D. Craig Miller, E. Kuhl, *J. Biomech.* **2011**, *44*, 1149.
[41] W. Bothe, E. Kuhl, J.-P.E. Kvitting, M.K. Rausch, S. Göktepe, J.C. Swanson, S. Farahmandnia, N.B. Ingels, D.C. Miller, *Circulation* **2011**, *124*.
[42] M. S. Sacks, Y. Enomoto, J. R. Graybill, W. David Merryman, A. Zeeshan, A. P. Yoganathan, R. J. Levy, R. C. Gorman, J. H. Gorman, *Ann. Thorac. Surg.* **2006**, *82*, 1369.
[43] K. Khoiy, D. Biswas, T. N. Decker, K. T. Asgarian, F. Loth, R. Amini, *J. Biomech. Eng.* **2016**, *138*, 111006.
[44] M. K. Rausch, W. Bothe, J. P. E. Kvitting, J. C. Swanson, N. B. Ingels, D. C. Miller, E. Kuhl, *Ann. Biomed. Eng.* **2011**, *39*, 1690.
[45] M. Walther, W. Bothe, M. K. Rausch, J. P. Escobar Kvitting, D. K. Echtner, M. Walther, N. B. Ingels, E. Kuhl, D. Craig Miller, *Circulation* **2012**, S231.
[46] M. K. Rausch, F. A. Tibayan, N. B. Ingels, D. C. Miller, E. Kuhl, *Ann. Biomed. Eng.* **2013**, *41*, 2171.
[47] M. K. Rausch, M. Malinowski, W. D. Meador, P. Wilton, A. Khaghani, T. A. Timek, *Cardiovasc. Eng. Technol.* **2018**, *9*, 365.
[48] M. Malinowski, A. G. Proudfoot, L. Eberhart, H. Schubert, J. Wodarek, D. Langholz, M. K. Rausch, T. A. Timek, *Int. J. Cardiol.* **2018**, *264*, 124.
[49] M. Malinowski, T. Jazwiec, M. Goehler, M. Quay, J. Bush, S. Jovinge, M. K. Rausch, T. A. Timek, *J. Thorac. Cardiovasc. Surg.* **2018**, *157*, 1452.
[50] C. E. Eckert, B. Zubiate, M. Vergnat, J. H. Gorman, R. C. Gorman, M. S. Sacks, *Ann. Biomed. Eng.* **2009**, *37*, 1757.
[51] A. G. Tsakiris, D. D. Mair, S. Seki, J. L. Titus, E. H. Wood, *Circul. Res.* **1975**, *36*, 43.

[52] K. A. Powell, L. Rodrigruez, P. Patwari, N. Greenberg, S. Chandra, D. M. Cosgrove, J. D. Thomas, *Comput. Cardiol.* **1994**, 353.
[53] M. E. Hiro, J. Jouan, M. R. Pagel, E. Lansac, K. H. Lim, H.-S. Lim, C. M. Duran, *J. Heart Valve Dis.* **2004**, *13*, 452.
[54] A. Basu, C. Lacerda, Z. He, *Cardiovasc. Eng. Technol.* **2018**, *9*, 217.
[55] K. Owais, C. E. Taylor, L. Jiang, K. R. Khabbaz, M. Montealegre-Gallegos, R. Matyal, J. H. Gorman, R. C. Gorman, F. Mahmood, *Ann. Thorac. Surg.* **2014**, *98*, 1536.
[56] H. Nishi, K. Toda, S. Miyagawa, Y. Yoshikawa, S. Fukushima, M. Kawamura, D. Yoshioka, T. Saito, T. Ueno, T. Kuratani, Y. Sawa, *Circ. J.* **2015**, *79*, 873.
[57] M. Malinowski, A. G. Proudfoot, D. Langholz, L. Eberhart, M. Brown, H. Schubert, J. Wodarek, T. A. Timek, *Interact. Cardiovasc. Thorac. Surg.* **2017**, *24*, 905.
[58] M. Malinowski, P. Wilton, A. Khaghani, D. Langholz, V. Hooker, L. Eberhart, R. L. Hooker, T. A. Timek, *Eur. J. Cardiothorac. Surg.* **2016**, *49*, 40.
[59] M. Malinowski, H. Schubert, J. Wodarek, H. Ferguson, L. Eberhart, D. Langholz, T. Jazwiec, M. K. Rausch, T. A. Timek, *Ann. Thorac. Surg.* **2018**, *106*, 1804.
[60] M. Stevanella, E. Votta, M. Lemma, C. Antona, A. Redaelli, *Med. Eng. Phys.* **2010**, *32*, 1213.
[61] D. Kamensky, F. Xu, C.-H. H. Lee, J. Yan, Y. Bazilevs, M.-C. C. Hsu, *Comput. Methods Appl. Mech. Eng.* **2018**, *330*, 522.
[62] F. Kong, T. Pham, C. Martin, R. McKay, C. Primiano, S. Hashim, S. Kodali, W. Sun, *Ann. Biomed. Eng.* **2018**, *46*, 1112.

How to cite this article: Rausch MK, Mathur M, Meador WD. Biomechanics of the tricuspid annulus: A review of the annulus' in vivo dynamics with emphasis on ovine data. *GAMM - Mitteilungen*. 2019;42:e201900012. https://doi.org/10.1002/gamm.201900012